

Investigation on Deposition of the Machined By-Products and Its Reduction during Electrochemical Discharge Machining (ECDM)

To cite this article: Rajendra Kumar Arya *et al* 2022 *J. Electrochem. Soc.* **169** 023506

View the [article online](#) for updates and enhancements.

You may also like

- [Computational modelling and experimental investigation of micro-electrochemical discharge machining by controlling the electrolyte temperature](#)
Dil Bahar, Akshay Divedi and Pradeep Kumar
- [Investigation of machining characteristics during micro-hole fabrication in CFRP composite by ECDM process](#)
Santosh Kumar Yadav, Abhishek Singh and Kishore Debnath
- [Enabling Jet-Electrochemical Discharge Machining on Niobium-Like Passivating Metal and the Single Step Fabrication of Coated Microstructures](#)
Jiajun Lu, Sanjun Liu and Yonghua Zhao



Your Lab in a Box!

The PAT-Tester-i-16: All you need for Battery Material Testing.

- ✓ All-in-One Solution with integrated Temperature Chamber!
- ✓ Cableless Connection for Battery Test Cells!
- ✓ Fully featured Multichannel Potentiostat / Galvanostat / EIS!

www.el-cell.com +49 40 79012-734 sales@el-cell.com


electrochemical test equipment





Investigation on Deposition of the Machined By-Products and Its Reduction during Electrochemical Discharge Machining (ECDM)

Rajendra Kumar Arya,^{1,z} Shivangi Paliwal,¹ Akshay Dvivedi,² and Rajakumaran Maran²

¹Mechanical Engineering Department, Indian Institute of Technology Bombay, 400076, India

²Mechanical and Industrial Engineering Department, Indian Institute of Technology Roorkee, Roorkee, 247667, India

Electrochemical action and subsequent discharges are utilized in electrochemical discharge machining (ECDM) for the fabrication of components by subtracting the undesired material. However, as the process progresses, localized electrolyte vaporization (machining zone) and its leading effects limit the process performance. Controlled delivery of fresh electrolyte into the machining zone to replenish the vaporized electrolyte improves the ECDM process performance, utilized in the electrolyte injection-ECDM (EI-ECDM) process. Apart from the control strategies, the literature lacks a detailed investigation of the phenomena involved in deteriorating the ECDM's machining performance. Few researchers enlighten that the deposition of the machined by-products on the tooltip might be a significant reason. Therefore, the present work is carried out to investigate the influence of deposition of the machined by-products on outcomes of the ECDM process at different parametric conditions. Various scientific tools and techniques are used to explore the underlying phenomena of machined by-products deposition. It shows that deposition significantly alters the geometry, surface texture, and properties of tool-electrode, which intern affects the ECDM's performance. Further, experimental results and subsequent characterization reveal that EI-ECDM can significantly control the deposition and enhance the process performance. Thus, a multi-response optimization was performed to increase the applicability of the EI-ECDM process.

© 2022 The Electrochemical Society ("ECS"). Published on behalf of ECS by IOP Publishing Limited. [DOI: [10.1149/1945-7111/ac4f6f](https://doi.org/10.1149/1945-7111/ac4f6f)]

Manuscript submitted September 30, 2021; revised manuscript received December 14, 2021. Published February 17, 2022.

Electrochemical Discharge Machining (ECDM) has been emerging as a promising micro-machining process for the last couple of decades, particularly for non-conductive materials. The main reason is its flexibility to machine a wide range of hard-to-machine materials such as quartz,¹ glass,² superalloys,³ carbon epoxy composites,⁴ metal matrix composites,⁵ etc. This process has proved its capabilities to fabricate micro features, especially on non-conducting materials like glass and ceramic.^{6,7}

ECDM is an apposite paradigm of the hybrid micromachining technique. It blends the characteristic features of electrochemical machining and electro-discharge machining. The ECDM process embraces electrolytic bath (i.e., aqueous electrolyte solution), DC pulsed power supply, work material, two electrodes (i.e., tool-electrode, which generally act as a cathode and auxiliary electrode anode). The tool-electrode is kept immersed up to 1.5–2 mm into the electrolyte bath, and work material is placed beneath the tooltip and wholly immersed in the electrolyte. Similarly, the auxiliary electrode is entirely immersed in the electrolytic bath. Thus, it forms an electrolytic cell circuit (ECC), wherein the process of electrolysis occurs as the DC voltage is supplied to both the tool-electrodes by using a DC pulsed power source.² The electrolysis in ECC results in the production of hydrogen gas from the immersed surface of tool-electrode, and oxygen gas from the auxiliary electrode.⁵ Furthermore, these H₂ gas bubbles gather around the tool-electrode and thus create a dielectric gas film by coalescence of H₂ bubbles.⁸ This gas film acts as an obstruction in the path of current flow between the tool-electrode and electrolyte interface. This resistance in the current flow also initiates the phenomenon of joule heating in the ECC and causes the formation of vapor bubbles altogether with electrolyte vaporization.⁹ Similarly, the resistance of tool material can accelerate the phenomena of joule heating. Subsequently, these vapor bubbles combine with hydrogen gas bubbles to form enlarged gas bubbles around tool-electrode, leading to thick gas film formation. Wuthrich et al. (2014) advocated the same that in-addition to the H₂ gas bubbles, localized electrolyte evaporation due to the phenomenon of joule heating is equally responsible for gas film formation.¹⁰ Therefore, a sudden drop of current due to increased resistance increases the current density inside gas film formed around tool-electrode. It causes intensified electric field generation, leading to electrochemical discharge (plasma) between tool-electrode and work material (i.e., machining zone) by breakdown of H₂

gas film around tool-electrode.^{6,8,11} Thus, the thermal energy generated due to the consistent discharges around the tool-electrode is particularly desired at the tooltip for efficient and high-quality machining outcomes. In ECDM, the electric discharges primarily contribute to the material removal from work via melting and evaporation, followed by fast-tracked high-temperature chemical etching.¹² However, at the same time, it vaporizes the localized electrolyte around the tooltip and the machined by-products (i.e., sludge, salt, and debris) remains within the machining zone.² Over the years, some researchers have focused on resolving this issue by improving the localized electrolyte flow to the tooltip. Some of the work is discussed below.

In the last few decades, a handful of researchers have been incorporated an additional energy source with ECDM phenomena to fulfill the electrolyte deficiency in the machining zone (at tooltip). Similarly, few others have used tool rotation; wherein, the centrifugal force enhanced the localized electrolyte flow during ECDM. In another investigation, Arya and Dvivedi (2019) quantified the electrolyte evaporation rate at various thermal energy inputs.² They further replenished the vaporized electrolyte by injecting the fresh electrolyte (also called pressured electrolyte flow) into the machining zone through a tubular tool-electrode during the ECDM process. Eventually, they reported the deepest microhole on borosilicate using the developed process.

On the other hand, literature has also revealed the importance of tool-electrode geometry and properties during microfabrication using the ECDM process. Flat side wall tool, coated tool, spherical tip tool, tube-shaped, and drill bit shaped tool have been primarily investigated.^{6,13,14} The multi-tip tool electrode was also utilized to fabricate through-glass vias by Kanno et al. (2019).¹⁵ Literature on tool properties shows that Mousa et al. (2008) determined the role of thermal conductivity of tool-electrode during gravity feed micro-drilling.¹⁶ Yang et al. (2010) investigated that wettability is one of the pivotal elements affecting the gaseous film structure.¹

It has been observed that the available literature mainly focused on enhancing the ECDM process performance by utilizing various methods. However, dedicated research is not found to investigate the phenomena causing the localized electrolyte vaporization and formation of the machined by-product, which can be a significant contribution to exploring the critical deposition phenomena during the ECDM process. Some researchers enlighten joule heating causes localized electrolyte heating and vaporization.¹⁰ As a fact, joule heating occurs due to the electrical circuit's resistance and increases with higher resistance. Hence, in the ECDM process, alteration in

^zE-mail: aryarajendra10iitr@gmail.com

tool electrical resistance can strongly affect the joule heat, and finally, the process performance.

Researchers have noticed that the machined by-products formed during machining accumulate in the machining zone and are deposited on the tool tip. Thus, it can affect the tool texture, shape, and properties, subsequently, the process performance of the ECDM process. Behroozfar and Razfar (2016) performed experimental work to characterize the tool wear on various tool materials during ECDM of the refractory materials.¹⁷ They had shown the deposition of debris and resolidified particles on the tool surface at high voltage and electrolyte concentrations. Sabahi and Razfar (2017) used mixed electrolytes and characterized the tool electrode before and after machining.¹⁸ Mishra et al. (2019) also showed the deposition of by-products on the tool after machining.¹⁹ However, all the published works only shed light on this issue of the ECDM process; a thorough investigation of machined by-products deposited on the tool tip and its consequence can further explore the ECDM machining mechanism. The obtained information regarding deposition may also be helpful for analyzing the process performance of the conventional as well as modified ECDM process. Therefore, the present work mainly focused on analyzing the machined by-products deposition on tool-electrode during ECDM and electrolyte injection-ECDM (EI-ECDM) process. The experiments were performed to investigate the implication of machined by-products deposition (on the tool-electrode tip) on ECDM performance during the fabrication of holes on borosilicate glass. Reduced deposition on the tool-electrode using controlled electrolyte injection during the EI-ECDM process was also revealed, which improved the process outcomes. FE-SEM, EDX, and image processing techniques were used to explain the underlying phenomena and estimate the percentage deposition of machined by-products on tool-electrode. Further, the effect of applied voltage, pulse-on-time (T_{on}), electrolyte concentration on percentage deposition on tool-electrode was discussed. The obtained results were also correlated with other process outcomes such as hole-over-cut (HOC) and hole-penetration-depth (HPD).

Material and Methods

Experimental setup.—An in-house developed setup of the Electrolyte Injection-ECDM (EI-ECDM), shown in Fig. 1, was used to perform experiments.² This setup was explained meticulously in the published work by Arya and Dvivedi (2019). The EI-ECDM setup comprises of pulsed type DC power supply, closed-loop tool feeding system (CLTFS), electrolyte chamber, work

material fixture, electrolyte-injection system, two electrodes (tool and auxiliary electrode), mounting tool unit, three linear axes (XYZ-axes). Herein, X and Y-axis were utilized to hold the electrolyte chamber, and the motion in Z-axis was employed to progress the drilling activity through displacing tool-electrode. The CLTFS provides adaptive tool-electrode feeding (developed to provide better control over the stochastic nature of the ECDM process²), and it comprises a force sensor, controlling unit, and Z-axis. Herein, a Z-axis stepper motor was connected to a microcontroller through a motor drive (both are employed in the controlling unit). Thus, the microcontroller's preloaded program controlled the tool's up/down motion through the feedback signals (i.e., generated from a force sensor). This force sensor (Model: FSG15N1A, Make: honey well, India), having a resolution of 1 g force, was physically connected to the work material fixture. Hence, it would sense the infinitesimal contact between work material and tool-electrode, which in response gave rise to force signals. The microcontroller received these force signals and instructed the motor driver to control the tool's motion and position through the commands on the preloaded program. In this program, a threshold value of force was written to instruct the motor driver. If, the current value < threshold value, the tool moved towards the work-material to fill the gap created due to material removal, else the tool retrieved back until it forms a predefined working gap between tool and work-material. This action was eventually taken to prevent the tool bending or/and work material damage.

A dial gauge (model: RYV 327, Mitutoyo, Japan), having a resolution of $1\ \mu\text{m}$, was used to measure the working gap as well as the hole penetration depth. The programmable pulse DC power supply (Model: SM 330-AR-22, Make: DeltaElektronika, Netherlands) was employed to provide the potential difference in the ECC. The syringe pump was used to inject a precise amount of fresh electrolyte into the machining zone using a 20 ml syringe.

A stainless steel (SS-304) tube, comprising 8%–10% nickel (Ni) and 18%–20% chromium (Cr), of inner diameter $310\ \mu\text{m}$ and outer diameter of $600\ \mu\text{m}$, was chosen as tool-electrode in experiments. The tool-electrode and auxiliary electrode were connected to the negative and positive terminal of the DC pulsed power supply, respectively. The graphite ring with an inner diameter of 8 cm, an outer diameter of 10 cm, and a thickness of 1.5 cm was utilized as auxiliary electrodes. It was placed at the base of the electrolyte bath. Thus, it submerged into the electrolyte bath. The borosilicate glass was selected as a work material. Aqueous NaOH was preferred in the ECDM process.^{2,6,20} Hence it was used as an electrolyte medium.

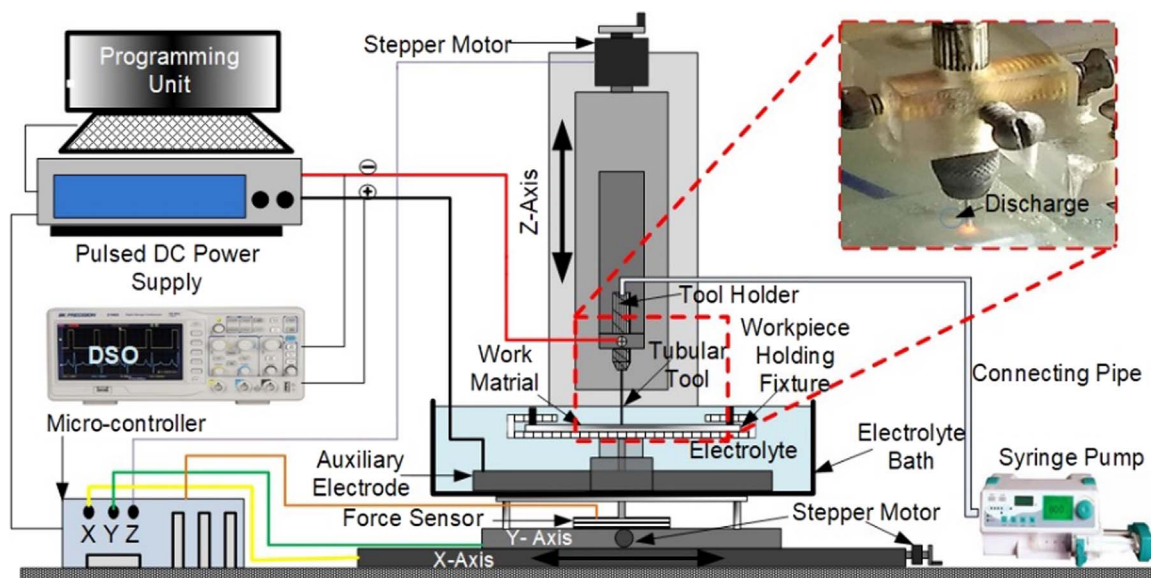


Figure 1. Schematic view of electrolyte injection-ECDM (EI-ECDM) setup.

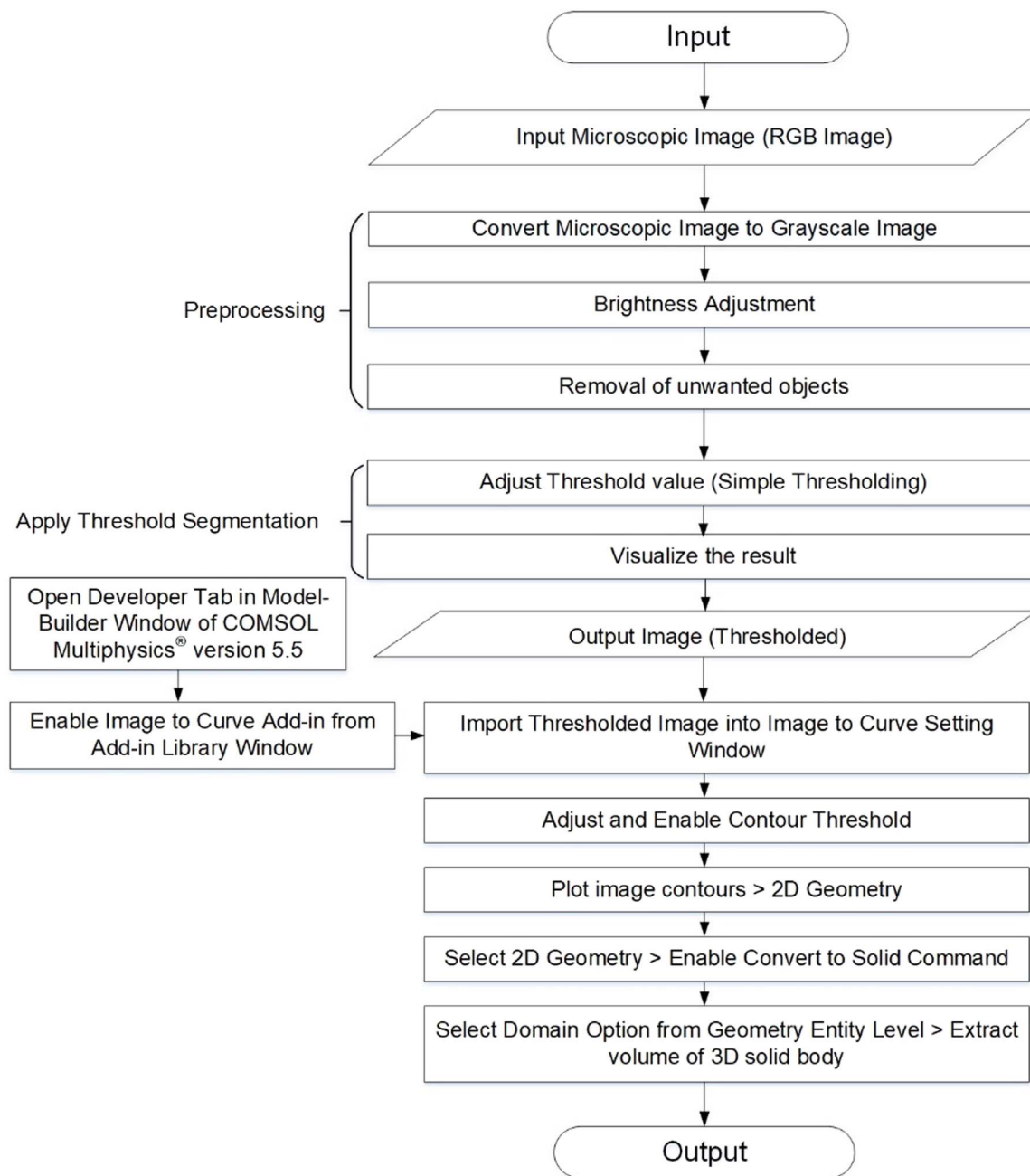


Figure 2. Algorithm for image processing.

Measurements.—The morphology of bare and used tool-electrode was characterized using a stereo zoom microscope (SMZ745 T, Make: Nikon). Subsequently, the obtained microscopic images were processed on ImageJ (Version 1.53D) and COMSOL Multiphysics® version 5.5 software to compute the volumetric deposition of machining by-products over the tool-electrode tip after machining. The method to estimate the volumetric deposition is presented in the subsection. Finally, the computed volumetric deposition (in percentage change in volumetric deposition) was also selected as a third process outcome to evaluate the process performance. This percentage change in a volumetric deposition was computed as:

$$\text{Deposition}(\%) = (V_{UT} - V_{BT})/V_{BT}$$

where, V_{BT} is the volume of the tool-electrode before machining (i.e., bare tool-electrode) and V_{UT} is the volume of tool-electrode after machining or using tool-electrode.

Furthermore, the performance of ECDM and EI-ECDM were evaluated by measuring hole-penetration-depth (HPD) and hole-overcut (HOC) on the fabricated holes. Also, the results of HOC and HPH were correlated with the percentage deposition results. The HPD was measured with the aid of a dial gauge (Model: 2109S-10, Make: Mitutoyo, Japan), having the least count of $1\ \mu\text{m}$. For measuring the HOC, microscopic images of the drilled holes were captured from a stereo zoom microscope, where HOC is calculated as,

$$\text{HOC} = 0.5(D_h - D_t)$$

Where, D_h is the diameter of the drilled hole at its entrance point, as measured with the help of a stereo zoom microscope and D_t is the outermost diameter of tubular tool-electrode (i.e., $600\ \mu\text{m}$).

Estimation of the volumetric deposition on the tool-electrode tip.—In the ECDM process, the machined by-products form during

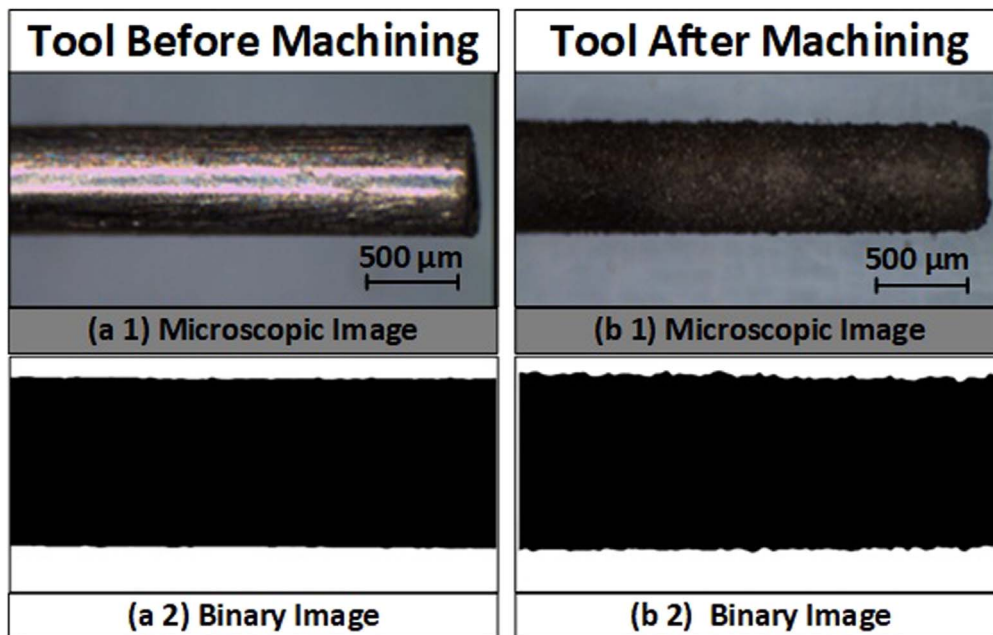


Figure 3. Microscopic images (a1) tool before machining, (b1) tool after machining, (a2) binary image of a1 image after thresholding, and (b2) binary image of b1 image after thresholding.

the machining operation, which further deposits on the tool-electrode tip. Literature reveals that this can affect the machining performance of the ECDM process by changing the physicochemical properties of the tool-electrode. Therefore, the volumetric change of tooltip due to deposition of the machined by-products in the tooltip was estimated. Image processing was performed using ImageJ (Version 1.53D) and COMSOL Multiphysics® version 5.5 software on the microscopic images of the tool-electrode. In this regard, the images of tool-electrodes (i.e., used at various machining conditions during ECDM and EI-ECDM) were captured from a stereo zoom optical microscope (SMZ745 T). An electromechanical system was used to hold and rotate the tool about a longitudinal axis for capturing the multiple images of the tooltip. The system was capable of precisely controlling the tool's angular position with a resolution of $<1^\circ$. Further, the captured multiple microscopic images were processed in image processing tools. The algorithm developed for image processing is given in Fig. 2.

Further, Fig. 3 shows the captured microscopic images of the tool-electrode tips, which were imported and processed on ImageJ (Version 1.53D) to obtain the binary images. The actual microscopic images and the binary images of tool-electrodes (a1–a2) before machining and (b1–b2) after machining, respectively, are depicted in Fig. 3. Here, irregularities on edges can be observed on a binary image of tool-electrode after machining. The obtained binary images were further processed in the Modeler window of COMSOL Multiphysics® version 5.5 software to compute the change in volume of the tool-electrode.

In COMSOL, the “contour threshold” command was used to create a sharply outlined region of bare tool-electrode and the deposition on used tool-electrode. The sequence of operations (i.e., illustrated in Fig. 4) was used to obtain a 3D model, which was further utilized to estimate the volume of a tool-electrode tip. This method was mainly used to estimate the volume of deposition (i.e., machined by-products) overlaid over the tool-electrode. Here, the volume of the bare tooltip and used tooltip was calculated. Eventually, the deposition volume was determined by subtracting the bare tooltip's volume from the used tooltip's volume (added deposition layer over the bare tool).

Experimentation Details

Pilot experimentation.—Available literature depicts that the ECDM performance deteriorates after a certain duration of machining operation. The primary reasons are localized electrolyte vaporization and the formation of the machined by-products.¹⁸ It can lead to the deposition of machined by-products on the tooltip, which may further cause a lowering of the machining performance of the ECDM process. Also, a recently utilized electrolyte injection through tubular tool-electrode with precise control was found as a scientific solution to enhance the ECDM process's performance by replacing the vaporized electrode. In this work, the process refers to electrolyte injection-ECDM (EI-ECDM) which is further explored to understand the effect of deposition on process performance. Thus, the pilot experiments were conducted with the aim to obtain the percentage volume of deposition on the tool-electrode and to discuss its effect with respect to time on the process outcomes of the ECDM and the EI-ECDM process. One-factor-at-a-time (OFAT) approach was adopted for the experiments. OFAT is a preferable experimental approach to ascertain the effect of individual process parameters. Various researches have used this approach, wherein the behavior of the process in terms of process performance can be described by changing the value of one process parameter at a time.^{14,21} The process outcomes were evaluated by hole-over-cut (HOC) and hole-penetration-depth (HPD). In the meanwhile, except machining time, all the other process parameters like voltage of 54 V, electrolyte concentration of 20 wt%, pulse on time (T_{ON}) of 6 ms, pulse off time (T_{OFF}) of 1 ms, and electrolyte flow rate (EFR) of 4 ml h⁻¹ (for EI-ECDM process) were kept constant.

In order to comprehend the role of machining time, three discrete-time values were selected for experimentations. Figure 5 depicts the variation in percentage deposition with respect to machining time. Figures 6a and 6b show the effect of machining time on HOC and HPD, respectively. As can be seen in Fig. 5, the percentage of deposition of machined by-products increased by increasing the machining time. It is a well-known fact that the machined by-products increase with machining progression during the ECDM process because of the incessant localized electrolyte

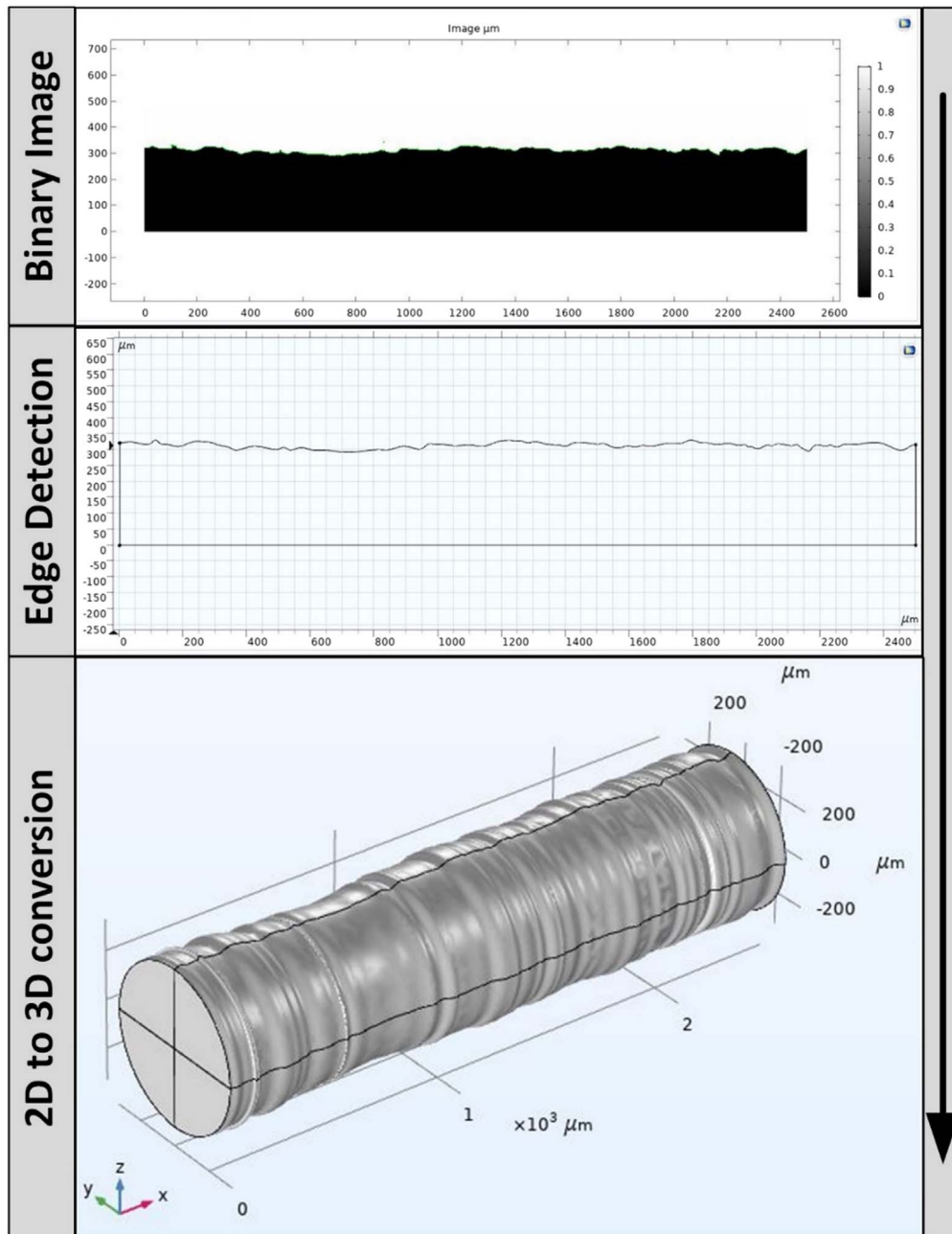


Figure 4. Sequence of steps followed in evaluating 3D volume of tool-electrode.

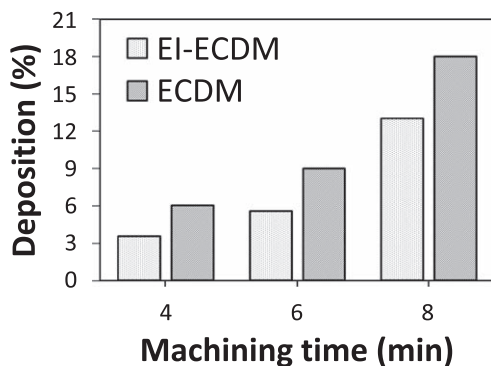


Figure 5. Effect of machining time on percentage deposition over tool-electrode.

vaporization. Thus, in the EI-ECDM process, providing controlled and continuous fresh electrolyte injection lowered the deposition percentage compared to the conventional-ECDM process. It can also be observed from Fig. 5 that the deposition gradually increased till 6 min. After that, it increased sharply. Similarly, increasing the machining time increased the HOC and HPD because of the increased periods of imparting discharge energy in the machining zone, as can be referred from Figs. 6a and 6b. However, increasing HOC is undesired for machining, but it is an unavoidable phenomenon in the ECDM process. Thus, quality machining can be considered the best possible HPD with acceptable HOC,^{2,12} obtained at 6 min machining time. Beyond it, the HOC increased abruptly with limited growth on HPD. A possible reason was found in Fig. 5, where the sudden rise was seen at 8 min of machining time. Excessive deposition due to a longer duration of electric discharges led to the formation of immense machined by-products at the tooltip

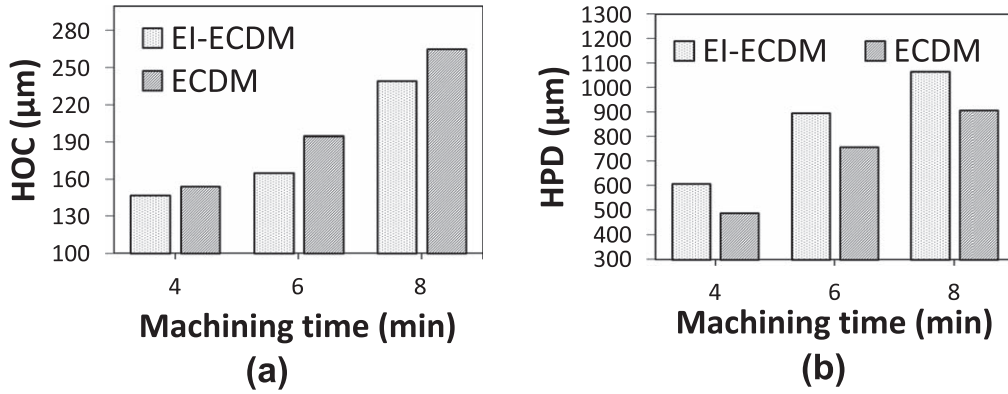


Figure 6. Effect of machining time on (a) HOC and (b) HPD.

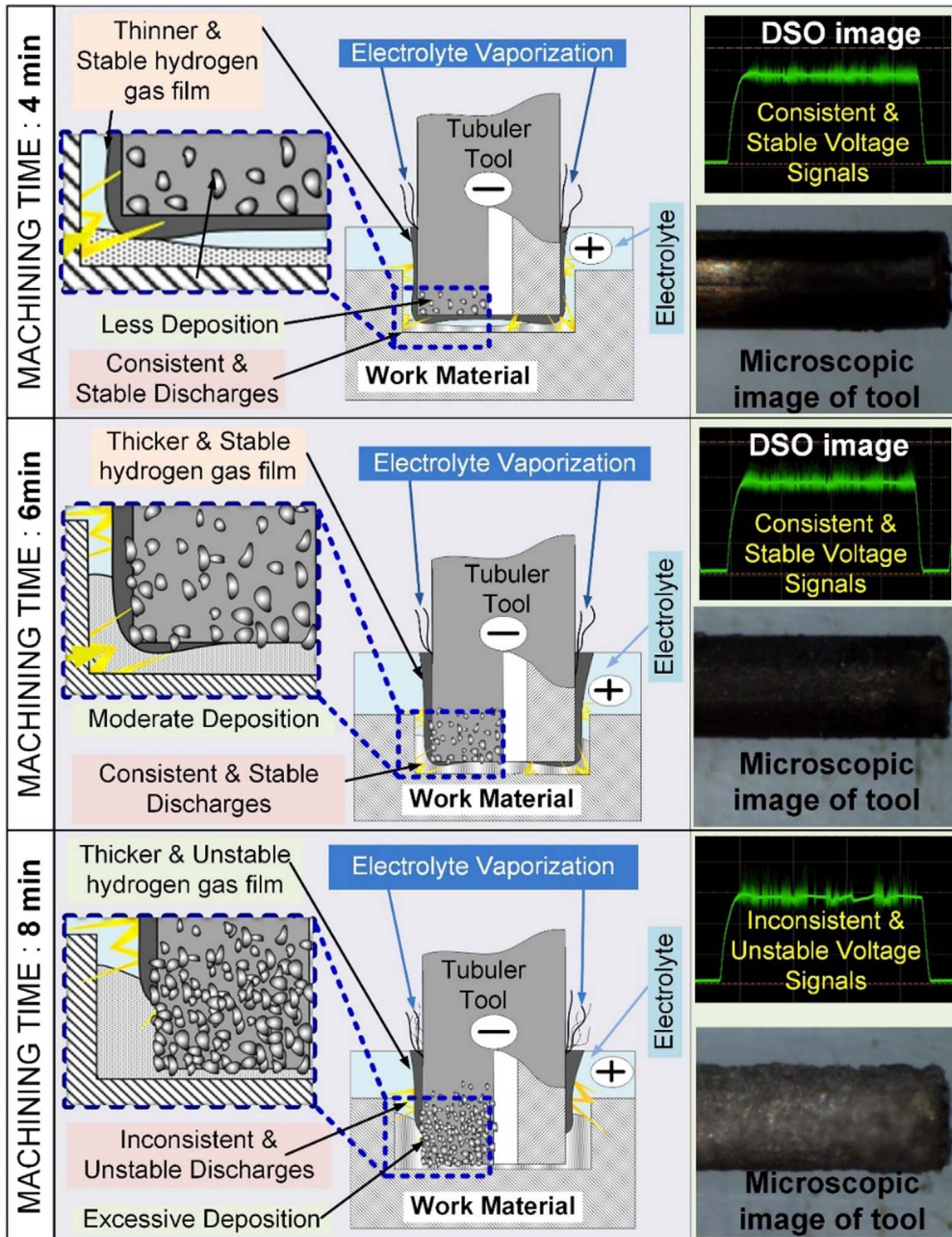


Figure 7. Phenomena of the machined by-product deposition with respect to machining time supported by DSO and microscopic images.

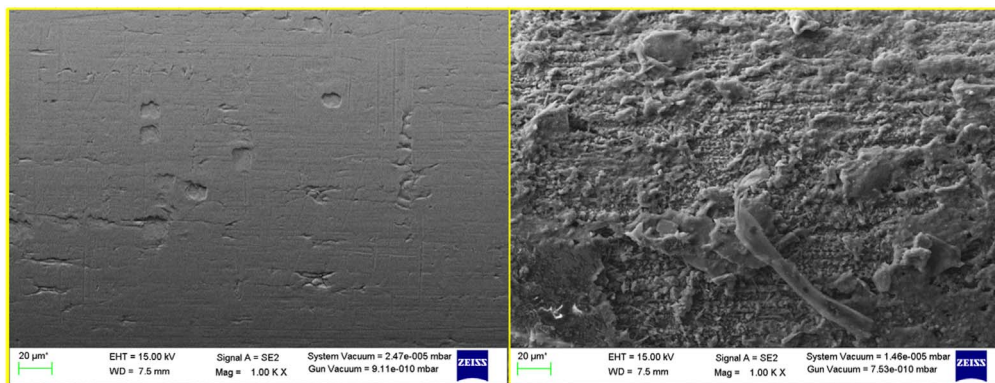


Figure 8. FE-SEM images of bare tool-electrode (before machining) and used tool-electrode (after machining).

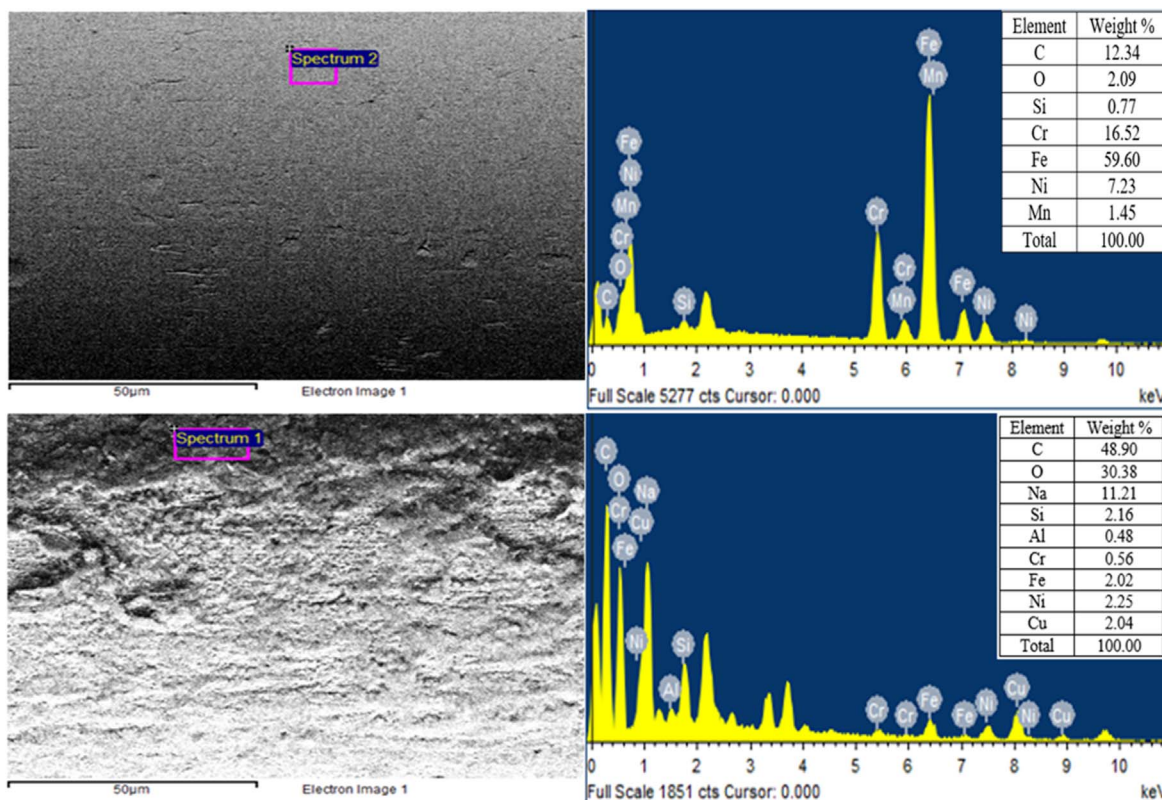


Figure 9. EDX spectra of (a) bare tool-electrode and (b) used tool-electrode.

(i.e., in the machining zone). Meanwhile, from Figs. 6a and 6b, it can also be observed that providing electrolyte injection in the EI-ECDM process improved the process and reduced the deposition of machined by-products on the tool surface. The reason thereof was that providing continuous electrolyte injection with precise control maintained the availability of electrolyte as well as its concentration inside the machining zone. It also lowered the accumulation of machined by-products inside the machined zone during the EI-ECDM process.

The above discussion revealed that the deposition of machined by-products on tooltips increases with an increase in machining time and significantly affects both the process's machining outcomes (i.e., HOC and HPD). Thus, based on the above discussion, a hypothesis was proposed to understand the phenomenon involved with machined by-products disposition on tooltips and its effect on machining performance. Further, the hypothesis was supported by experimental and image processing analysis.

Figure 7 shows a schematic view of the phenomenon involved in machined by-products accumulation and disposition during the ECDM process at different machining times. The DSO images were also depicted to understand the discharge characteristics. As shown in Fig. 7, continuous machining resulted in the formation of machined by-products, which were deposited on the tool electrode surface. The primary reasons for the formation of the machined by-products can be noticed as vaporization of localized electrolyte, machining debris from removed work material, and partially by anodic dissolution due to electrochemical action. It is evident in the available literature that the temperature near the tool electrode is much higher and sufficient for rapid vaporization of the localized electrolyte.^{2,17,22} Thus, salt and sludge accumulate around the tool electrode with machining progress. Moreover, the anodic dissolution due to electrochemical action and removed work material by electrodischarge action results in debris formation. At the same time, electrically conductive debris formed by anodic dissolution

contaminates the electrolyte and increases electrolyte's electrical conductivity during ECDM.¹⁸ Although increased conductivity initially accelerates material removal; however, high contamination limits the material removal by contributing to the accumulation of the machined by-products. Meanwhile, the oxidation and properties of electrolyte (which may change during machining) are dominating phenomena during ECDM of conductive materials due to significant electrochemical action.²³ Though in the present work, the work material was glass (non-conductive); thus, effects were not considered.

Eventually, it can be stated that the machined by-products such as salt, sludge, and debris accumulate inside the machining zone and deposit on the tool electrode surface. Some researchers have noticed that the flushing methods can help to remove the deposition of machined by-products.^{23,24} Hence, it can be stated that the possibility of formation of atomic, covalent, metallic or any other type of bonding is very unlikely between the machined by-products and tool electrode or the deposited machined by-products have just temporarily adhered to the tool electrode which can be easily removed. Besides, the bonding is possibly due to the Van Der Waals forces.

It can be observed from Fig. 7, a thick layer of the machined by-products was deposited at higher machining time owing to the continuous formation of machined by-products. It can be evidenced in the captured microscopic images of the tool-electrode tip, shown in Fig. 7 at the corresponding machining time. Moreover, the schematic showed that at 4–6 min machining time, the charge transfer (i.e., discharge) from sharp edges of the tool electrode (i.e., inner and outer edges) owing to the high current density region. Thus, high-frequency and stable electric discharges were formed, evidenced by DSO images. However, beyond 6 min of machining time, inconsistent and unstable voltage signals were obtained owing to excessive accumulation of the machined by-products in the machining zone and their disposition on the tool electrode surface. As a result, it formed a high current density region near the hole entrance instead of the tooltip. Subsequently, it formed a thick and unstable gas film at the hole entrance and generated low-frequency, high-intensity discharges (which can be seen from the DSO image at 8 min machining time). Thus, as a result, it deteriorated the ECDM process performance and resulted in poor outcomes (i.e., large HOC and lower HPD). It was observed in pilot experiments and can be seen in Figs. 6a and 6b. Further, the effect of deposited machined by-products hampers the performance of the ECDM process at higher machining time was demonstrated by FE-SEM and EDX analysis of tool-electrode tip.

The Field Emission Scanning Microscope (FE-SEM QUANTA 200 FEG, Make -FEI) equipped with energy dispersive X-ray (EDX)

was used in this study. The FESEM was performed to investigate the topography of the tool-electrode surface before and after machining. The EDX spectrometer was used to analyze the elements presented on the tool surface qualitatively. Meanwhile, gold sputtering in a high vacuum was done to the tool-electrode samples in order to improve their imaging.

Figure 8 illustrates the FE-SEM images of the bare tool-electrode and the used tool-electrode (after machining). Here, massive deposition of machined by-products (i.e., tool-electrode after 8 min machining time) can be easily observed. The immense hike in machined by-products deposition of low electrical conductivity elements reduces the active surface of the electrode and leads to a lower down electrical conductivity in the circuit. Hence, it seriously affects the ECDM process performance because a high electrical conductivity with better chemical internees is the essential property of tool-electrodes in the ECDM process. The tool-electrode of SS-304 material was used in the present work, which possesses both properties. Furthermore, the reduction in the electrical conductivity of the tool-electrode was confirmed by EDX analysis, explained in subsection.

The EDX was performed on the surface of bare tool-electrode and used tool-electrode to investigate the elements present on the tool surface. Moreover, the EDX results were utilized to estimate the tool electrode's electrical conductivity. Figure 9a depicts the weight % distribution of the various elements on the surface of the SS-304 tool-electrode (i.e., before and after ECDM). Here, it can be seen that Fe is the main constituent with a weight% of 59.60 because there are no external elements on the surface of the tool electrode. On the other hand, as the EDX was performed on the used tool, the Fe weight% drastically decreased to 2.02. It was due to the continuous deposition of by-products (i.e., glass debris, salt, and sludge) on the outer surface of the SS-304 tool electrode, which can be clearly seen in Fig. 8. It can be seen from Fig. 9b constituents due to the deposition of by-products are carbon, oxygen, and sodium. The fact of increasing the weight% of these constituents can be attributed to oxidation of debris and deposition of melted NaOH electrolyte due to vaporization of localized electrolyte.^{2,23} A similar observation was reported by Sabahi and Razfar (2017), where a massive deficiency in the tungsten (WC) tool and a significant increase in other elements was found.¹⁸

The EDX spectra of the used tool-electrode (Fig. 9b) show the presence of constituents like Na and Si, which can be associated with electrolyte and glass-substrate. Besides, an increased weight% of carbon and oxygen was observed in the deposited layer due to debris oxidation.²³ It may be due to the use of graphite as an auxiliary electrode in the ECDM circuit. Furthermore, we compared the

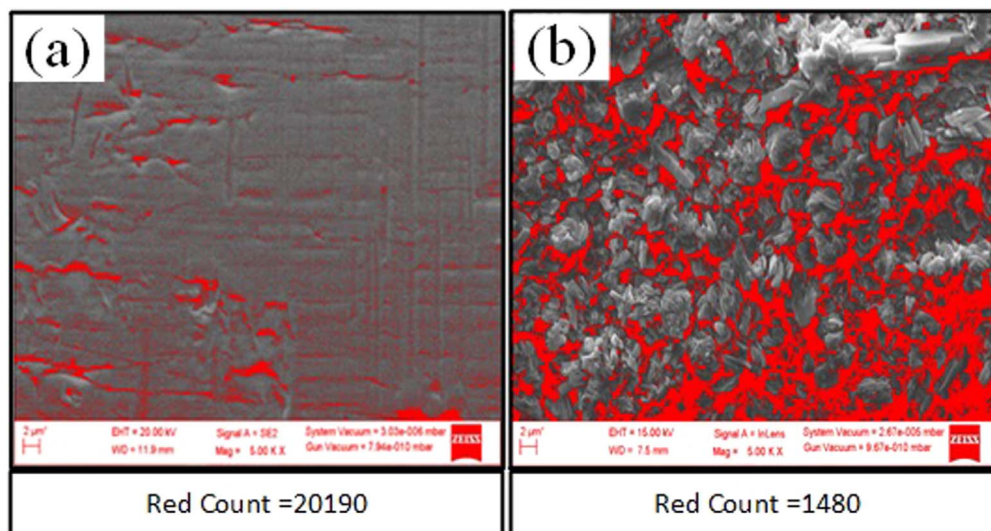


Figure 10. Estimation of nucleation sites on (a) bare and (b) used tool-electrode using ImageJ.

Table I. Process parameters and their specification.

Constant Process Parameter	Specification
Electrolyte bath	NaOH aqueous solution
Tubular electrode (Tool) material/Size (μm)	SS-304/600 OD and 350 ID
Anode (Auxiliary electrode)	Graphite
Work material/Size (mm^3)	Borosilicate glass slide/(75*25*1.35)
T_{off} (ms)	1
Machining time (min)	6
Variable process parameter	Range
Applied Voltage (V)	38, 46, 54, 62
T_{on} (ms)	2, 4, 6, 8
Electrolyte concentration (wt.%)	12, 20, 28
Electrolyte flow rate (ml h^{-1})	6

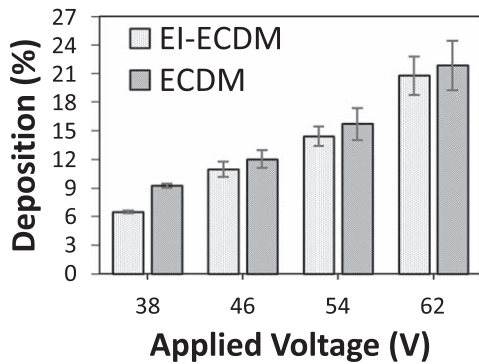


Figure 11. Effect of applied voltage on percentage deposition on the tool-electrode.

elemental composition of different elements on both the tool-electrodes. As a result, the variation in the atomic percent of elements like C, Si, Cr, Fe was diagnosed. Thus, the electrical conductivity of individual elements was evaluated from the periodic table, and later on, for comparison, the total electrical conductivity of bare tool and deposited layer on the used tool-electrode was estimated as per Eq. 1 with the purpose to determine the overall change in electrical conductivity.

$$\sigma_{eq} = \sigma_1 x_1 + \sigma_2 x_2 + \sigma_3 x_3 + \dots + \sigma_n x_n \quad [1]$$

where, σ = Electrical conductivity of the element
 σ_{eq} = Overall change in electrical conductivity of elements
 x = Atomic percentage of individual element

Using Eq. 1 the electrical conductivity of bare and used tool-electrode were calculated. Bare tool-electrode had $829.85 \times 10^6 \text{ S m}^{-1}$ electrical conductivity and it was reduced to $434.26 \times 10^6 \text{ S m}^{-1}$ in

used tool-electrode. In comparison, it is found that the deposited layer covering the tool-electrode during ECDM has lower electrical conductivity than that of the bare tool. The electrical conductivity is inversely proportional to the electrical resistance of the material.

In the above analysis, it has been noticed that constituents of the deposition layer can directly influence the resistance in the circuit. Meanwhile, it can be described by Ohm's law and Joule's first law.

Ohm's law says that the applied voltage V is a product of current I passed through a conductor and resistance R in the circuit, given in Eq. 2.

$$V = I \times R \quad [2]$$

Furthermore, as per Joule's law relation between generated heat Q and the resistivity is given as;

$$Q = I^2 \times R \times t \quad [3]$$

Equations 2 and 3 states that for a given applied voltage, an increase in the resistance (due to deposition) increases the joule heating around the tool electrode leading to rapid vaporization of localized electrolyte. In other words, the electrical energy converts into localized heating instead of electric discharges. The rapid evaporation of electrolyte with the progression of machining activity promotes the production of the machined by-products and their permanent deposition on the tool-electrode during ECDM. Eventually, it can be said that as the machining progresses, the electrolyte vaporization and machined by-products deposition increases each other and the cumulative effect of both worsens the ECDM process's performance.

Identification of nucleation sites on the tool-electrodes (i.e., bare and used tool-electrode).—In the ECDM process, the H_2 bubbles evolve from the nucleation sites on the tool-electrode.

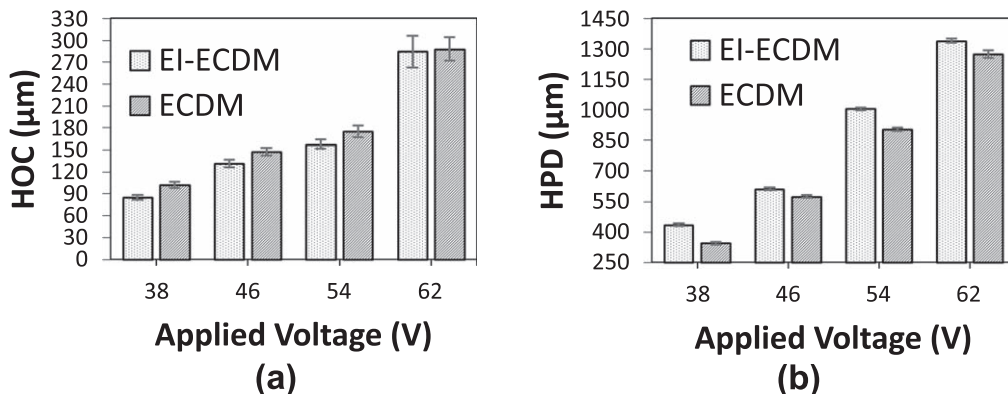


Figure 12. Effect of applied voltage on (a) HOC and (b) HPD.

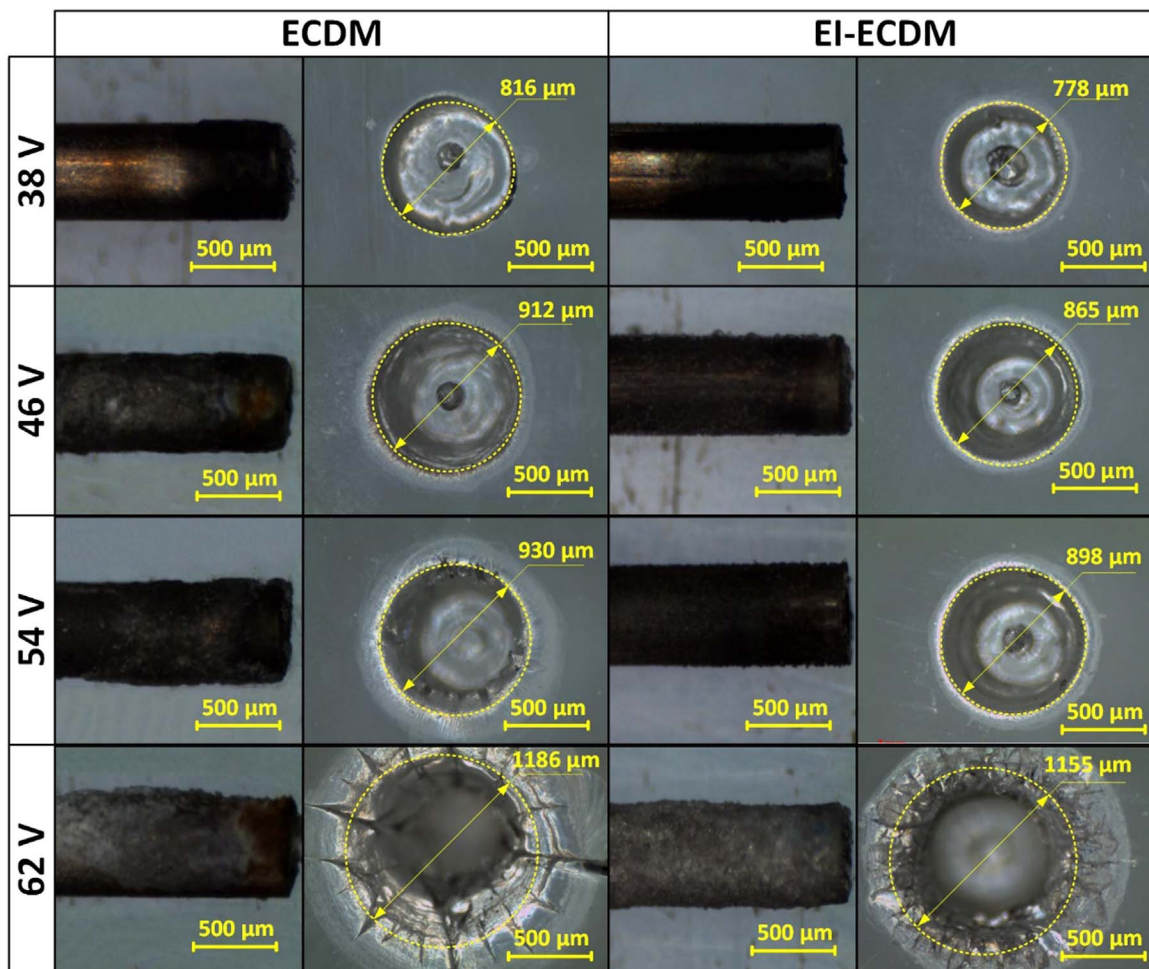


Figure 13. Microscopic images of used tool-electrode and fabricated holes at the different applied voltages using ECDM and EI-ECDM process.

Nucleation sites significantly affect the H_2 bubble formation process. Reduction in nucleation sites results in less bubble formation, thus deteriorating the H_2 gas film formation process and subsequent electric discharges. Eventually, it hampers the ECDM process performance. On the other hand, more nucleation sites provide thin and stable gas film by early coalescence of H_2 bubbles with the neighboring bubbles. Therefore, the images analysis was performed on the tool electrodes' SEM images (before and after machining). An image processing software, ImageJ (JAVA version) processing software, was used for the analysis. The threshold command with "Analyze Particles" was used to determine the number of cell counts in the software. For this purpose, the threshold value of 50 was given to analyze the difference in the number of cell counts in both images. Subsequently, the ImageJ analysis algorithm showed that the red cell counts on the bare tool-electrode surface were higher than the used tool-electrode surface, as illustrated in Fig. 10. The red counts denote the number of nucleation sites on the tool-electrode's SEM images. The dominating reason for lowering the nucleation sites can be attributed to the deposition of machined by-products on the tool-electrode surface during the machining. The primary reasons for the deposition of the machined by-products and their bonding with tool electrode surfaces have been discussed in previous sections.

Moreover, the literature reveals that chemical etching can also change the nucleation sites on the tool electrode surface during the ECDM process. However, the chemical etching phenomenon dominates the work material, hence negligible for tool electrodes. Besides, in the present work, the tool electrode was made of 304 stainless steel, which has high resistance to chemical action for a wide range of concentrations and temperatures.²⁵ Furthermore, the

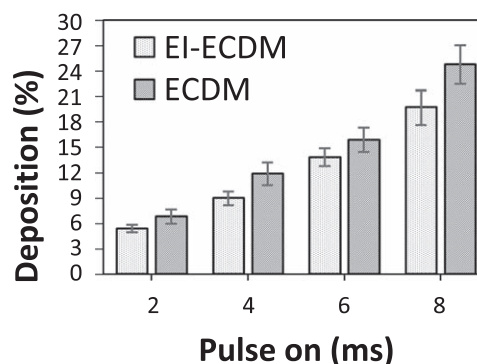


Figure 14. Effect of T_{on} on percentage deposition on the tool-electrode.

deposition of the machined by-products prevented the chemical etching of the tool electrode surface.

Experimental procedure.—The experiments were conducted to investigate the parametric effect on percentage deposition as well as the process outcomes (i.e., HOC and HPD) of the ECDM and EI-ECDM processes. Here also, the OFAT approach was used. The variable and constant process parameters are given in Table I. The methods to estimate the HOC and HPD have already been explained above. Each of the experiments at the same parametric setting was repeated three times. An average of HOC and HPD was considered a final result of the experiments, performed at various parametric conditions.

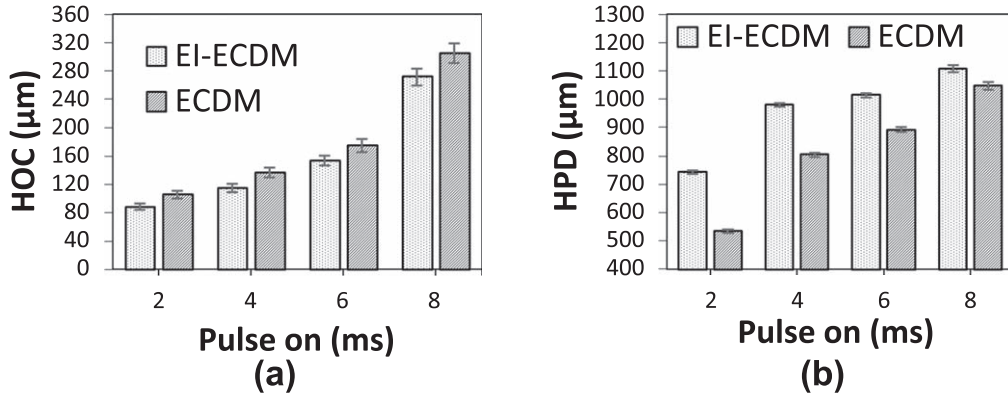


Figure 15. Effect of T_{on} (a) HOC and (b) HPD.

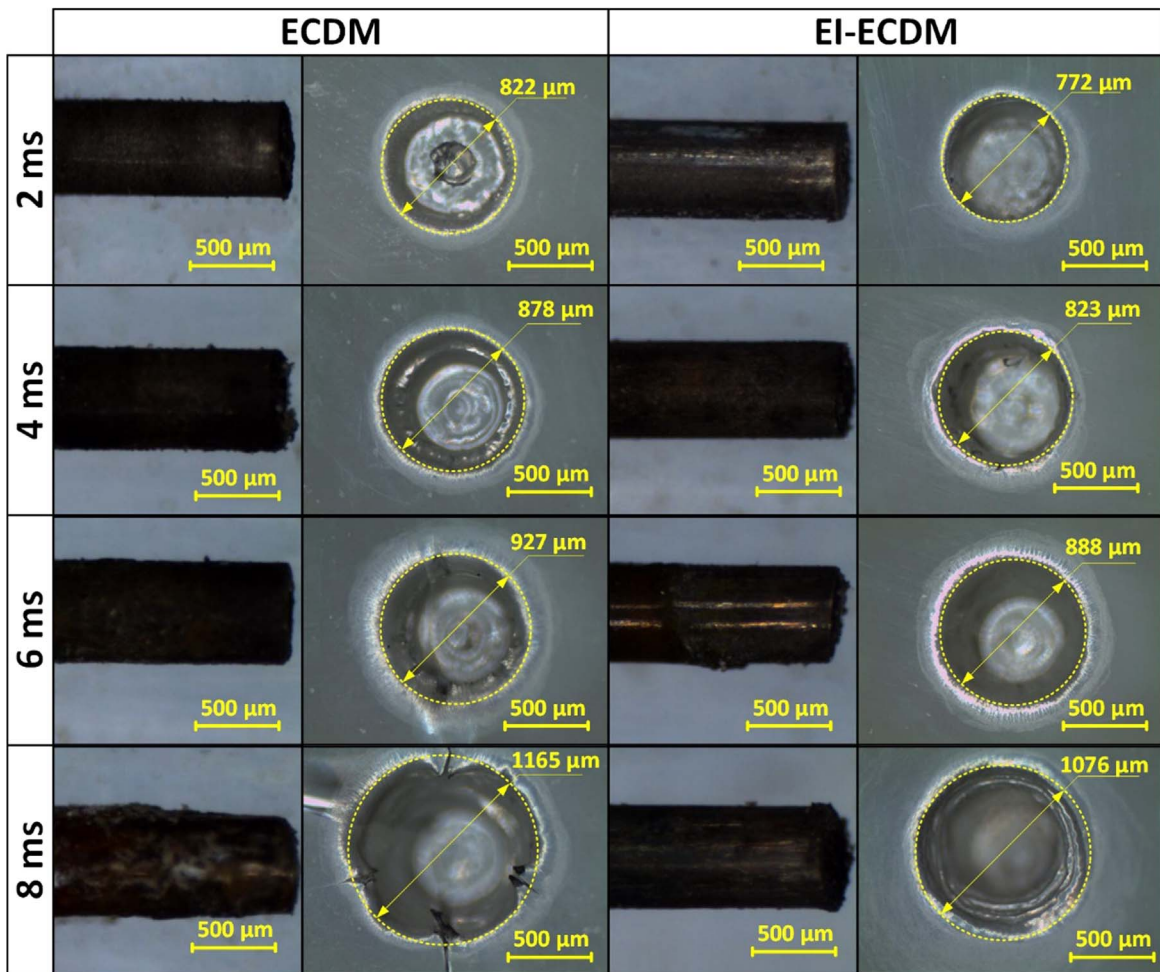


Figure 16. Microscopic images of used tool-electrode and fabricated holes at the T_{on} voltages using ECDM and EI-ECDM process.

Results and Discussion

This section presents the results of experiments conducted to understand the effect of various process parameters on the percentage deposition of machined by-products over the tooltip surface. Meanwhile, the experimental results also show the parametric effect and the obtained percentage deposition on HOC and HPD during the ECDM and EI-ECDM processes. The variable and constant process parameters used in the experiments are given in Table I.

Effect of applied voltage on machined by-products deposition and other process outcomes (i.e., HOC and HPD) of the ECDM

and EI-ECDM process.—Voltage is the decisive parameter, which governs the entire material removal mechanism of ECDM by controlling the energy input. The literature revealed that various investigations had been done to discuss the effect of applied voltage on multiple process outcomes such as material removal rate, tool wear rate, depth and hole diameter, etc. However, none of the published work has shown a quantification of machined by-products deposition on tool-electrode and its effect on other process outcomes at different applied voltages. Therefore, this section presents the experimental results of percentage deposition and other process outcomes (i.e., HOC and HPD) obtained at different applied

voltages. Meanwhile, the experiments were performed to compare the process performance of the ECDM and EI-ECDM processes at different applied voltages.

In experiments, the applied voltage was varied from 38 V to 62 V, while the other parameters such as machining time 6 min, electrolyte concentration 20 wt.%, T_{on} 4 ms, and T_{off} 1 ms were kept at their constant value. Besides, the electrolyte flow rate was maintained at 4 ml h^{-1} in all experiments for localized delivery of fresh-electrolyte into the machining zone in the EI-ECDM process. All the experiments were repeated three times in the same parametric condition.

The effect of applied voltage on the percentage deposition of machined by-products is shown in Fig. 11. It was noticed that percentage deposition on tool-electrode increased with an increase in applied voltage. A primary reason could be more localized electrolyte vaporization and machined by-products formation due to a rise in electrolyte temperature near the vicinity of tool-electrode at higher applied voltage. Hence, the EI-ECDM process resulted in less percentage deposition of machined by-products than the ECDM process by providing fresh-electrolyte into the machining zone (at the tooltip). At the same time, it can also be observed that the deposition percentage gradually increased up to the 54 V applied voltage. After that, an abrupt rise was observed in percentage deposition due to the excessive formation of the machined by-products under the immense discharge energy at 62 V applied voltage. The high imparted discharge energy caused rapid localized electrolyte vaporization followed by a large formation of the machined by-products.²² It can seriously affect the machining performance of both processes, which will be explored in the subsequent section.

Furthermore, Figs. 12a and 12b show applied voltage's effect on HOC and HPD during the ECDM and EI-ECDM processes. As observed, both HOC and HPD were increased at higher applied voltage because of the higher discharge energy. In the meantime, the HOC abruptly increased beyond 54 V applied voltage. The reason behind this can be attributed to the enormous deposition and accumulation of machined by-products at 62 V applied voltage, shown in Fig. 11. Earlier, it was illustrated in Fig. 7, excessive deposition of the machined-by products on tool-electrode deteriorates the ECDM process by generating inconsistent and unstable electric discharges. Besides, the electric discharges occur at the hole entrance instead of the hole bottom, lowering the HPD and increasing HOC. Apart from the inherent issue of forming the machined by-products during machining by the ECDM process, in the EI-ECDM process, providing fresh electrolyte injection at the tooltip enhanced the process performance for all values of applied voltages.

Improvement in the hole fabrication process and lower deposition of machined by-products for all the applied voltages using electrolyte injection can be evidenced in Fig. 13. This figure shows the microscopic images of the fabricated holes and used tool-electrodes at different applied voltages during ECDM and EI-ECDM. Massive deposition on tool-electrode and severe thermal damage with enlarged entrance diameter beyond 54 V applied voltage can be easily observed from Fig. 13. In the meantime, the hole's lower deposition and lower entrance diameter during the EI-ECDM process than the ECDM process can also be observed from the same figure. The thermal damage, cracks, and enlarged entrance diameter are undesirable for machining holes; thus, 54 V applied voltage was selected for further experiments.

Effect of pulse on time (T_{on}) on machined by-products deposition and other process outcomes (i.e., HOC and HPD) of the ECDM and EI-ECDM process.—In the ECDM process, a pulsed DC power supply is preferred for better machining process control. Control over the duration of pulse on time (T_{on}) with fixed pulse off time (T_{off}) is essential to minimize the thermal damage on a machined feature. Besides, it also improves the flushing of

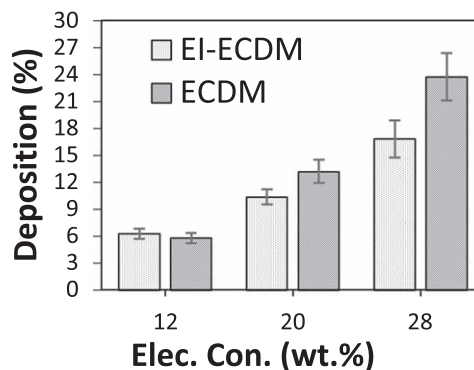


Figure 17. Effect of electrolyte concentration on percentage deposition on the tool-electrode.

machining by-products from the machining zone. Therefore, the subsection provides details of experimental results obtained at different T_{on} .

Initially, percentage deposition at different levels of T_{on} was obtained, followed by discussing the effect of T_{on} on HOC and HPD corresponding to the obtained percentage deposition. The experiments were conducted for 2–8 ms of T_{on} with 2 ms of interval. Other parameters such as machining time 6 min, electrolyte concentration 20 wt%/vol., applied voltage 54 V, and EFR 6 ml h^{-1} (in the EI-ECDM process) were set aside at a constant level during the experiments. Meanwhile, three experiments were performed at the same parametric condition to check the repeatability of the results. Figure 14 depicts that percentage deposition of machined by-products increased with increased T_{on} owing to the increased duration of discharging during machining. The increased machining duration increased the formation of the machined by-products leading to more deposition on tool-electrode.

In the following results (i.e., the effect of T_{on} on HOC and HPD), it was observed that increasing the T_{on} increased both the outcomes. The well-known reason was the prolonged discharging period for machining operations. However, the appreciable machining outcomes were achieved till 4 ms of T_{on} . Beyond 4 ms T_{on} , limited growth on HPD was obtained, and at the same time, the HOC increased rapidly. It was probably due to increased deposition on the tooltip at higher T_{on} (i.e., 6 and 8 ms), which led to the occurrence of electric discharges near the hole entrance instead of the tooltip. It was shown in Fig. 14 that increasing T_{on} increases the formation of machined by-products due to the increased discharging period. Thus, after a certain level of T_{on} , excessive formation of the machined by-products and its deposition on tooltip worsen the ECDM process and result in limited HPD with a large HOC, which can be noticed in Figs. 15a and 15b. Inconsistent and unstable electric discharges due to excessive deposition of machined by-products have been previously shown in the DSO image of Fig. 7.

In addition, the results in Figs. 15a and 15b also show that EI-ECDM provided better results over the ECDM process. Because of the lower deposition of the machined by-products on tool-electrode by sufficient supply of fresh-electrolyte to compensate the vaporized electrolyte. The lower deposition also reduced the Joule heating, followed by localized electrolyte vaporization and subsequent machined by-products formation. An appropriate discussion on electrolyte vaporization phenomena can be referred from the previous section (i.e., phenomena of deposition). Further, the experimental results were supported by microscopic images of machined holes and used tool-electrodes. Referring to Fig. 16, it clearly show that the EI-ECDM process enhanced the quality of holes in all the levels of T_{on} by maintaining the electric discharges at the tooltip owing to less deposition (shown in Fig. 14). However, at the peak level of T_{on} (i.e., 8 ms), the hole quality was inferior due to excessive deposition. It can be observed in the microscopic images

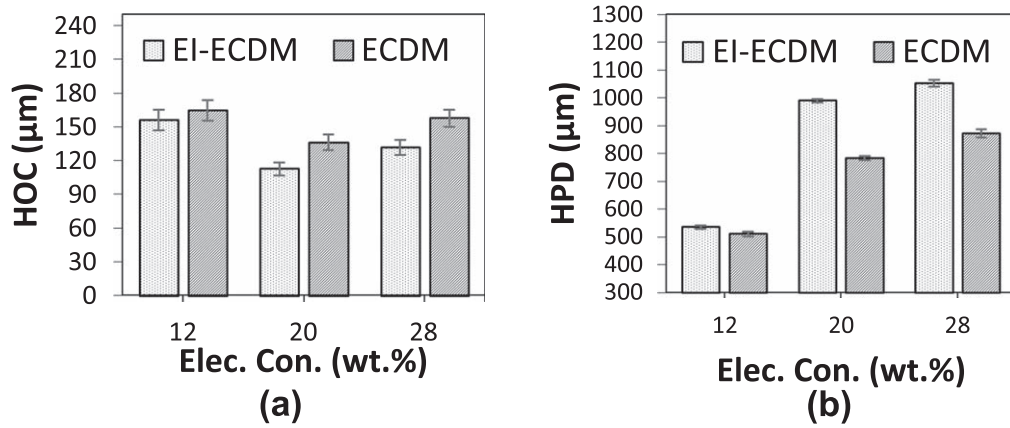


Figure 18. Effect of electrolyte concentration on (a) HOC and (b) HPD.

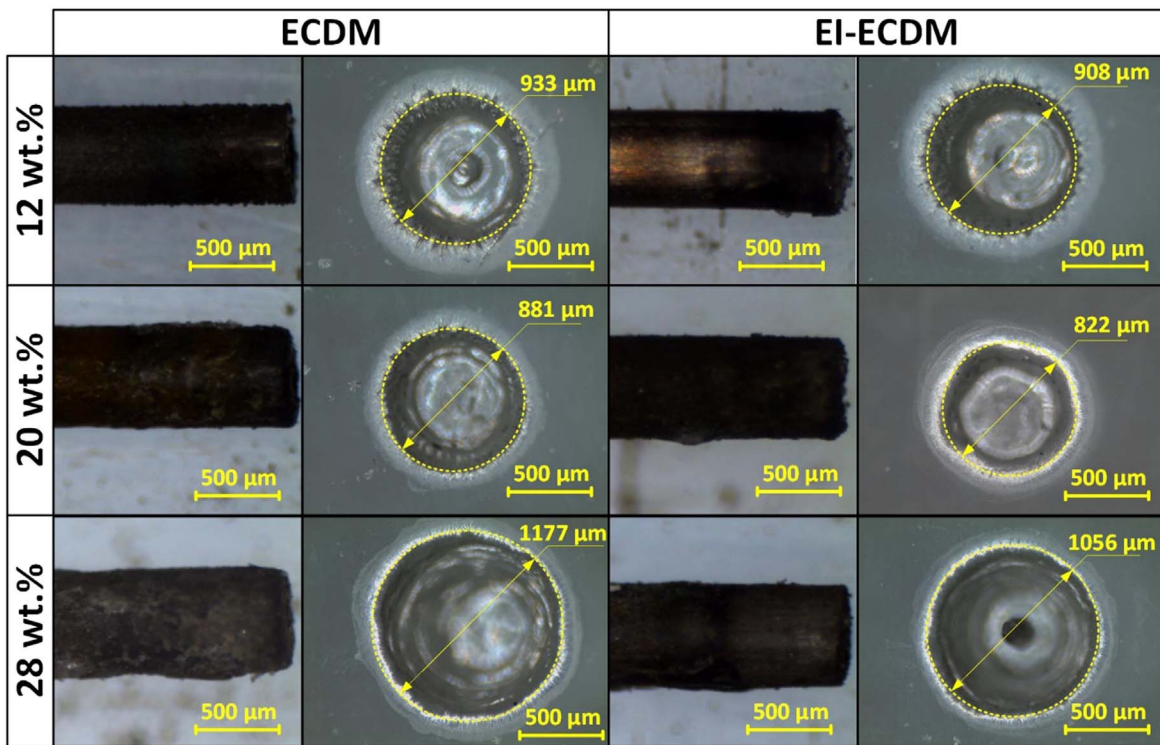


Figure 19. Microscopic images of used tool-electrode and fabricated holes at the T_{on} voltages using ECDM and EI-ECDM process.

Table II. The experimental results of EI-ECDM.

	Parameter value	Avg. Deposition (%)	Avg. HOC (μm)	Avg. HPD (μm)
Applied Voltage (V)	38	6	85	436
	46	11	132	612
	54	14	158	1005
	62	21	285	1340
Ton (ms)	2	5	88	743
	4	9	115	979
	6	14	154	1014
	8	20	272	1108
Electrolyte Concentration (wt.%)	12	6	156	536
	20	10	113	989
	28	17	132	1052

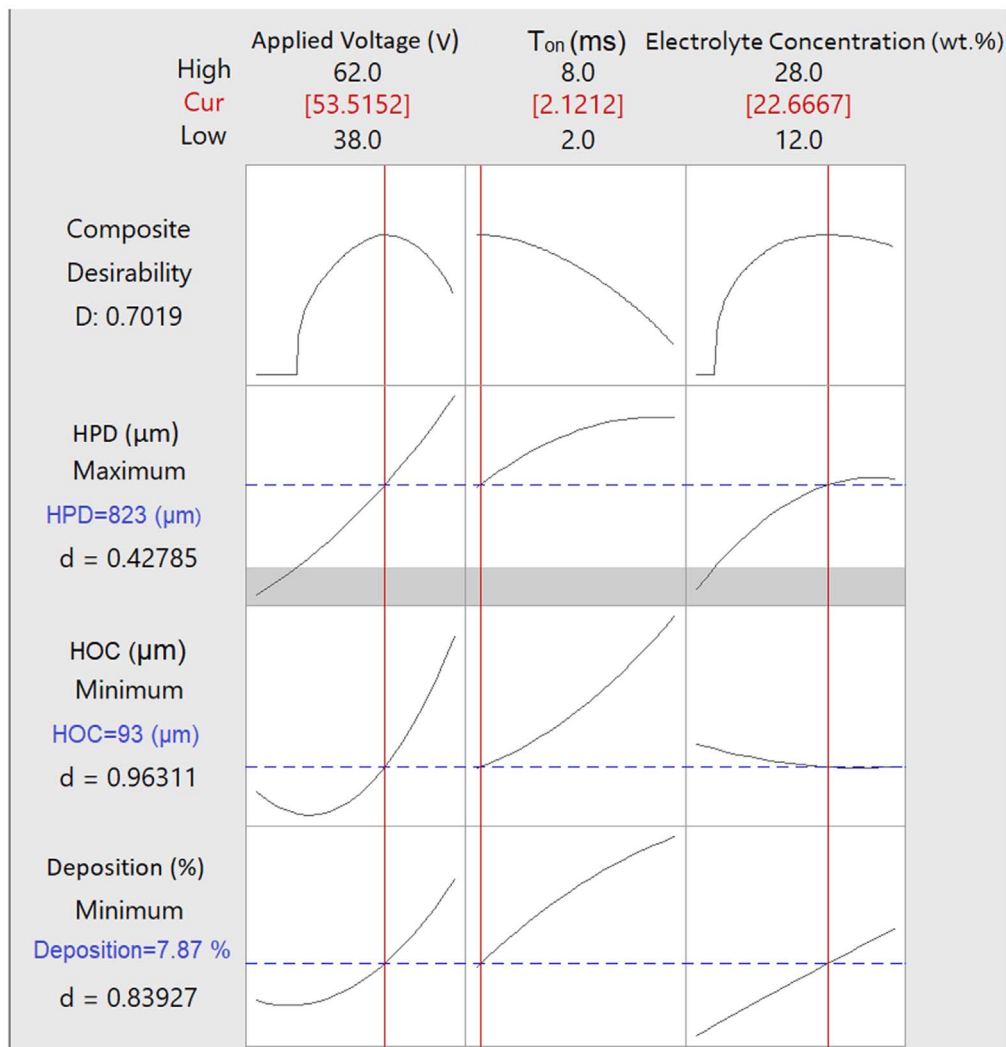


Figure 20. MRO results of the EI-ECDM responses.

of holes and corresponding tooltips. Limited progress in HPD with enlarged HOC beyond 4 ms T_{on} restricted to choose the 4 ms T_{on} for subsequent experiments.

Effect of electrolyte concentration on machined by-products deposition and other process outcomes (i.e., HOC and HPD) of the ECDM and EI-ECDM process.—It is imperative to investigate the effect of electrolyte concentration in the ECDM process because it governs conductivity and high-temperature chemical matching. Both play a vital role in the material removal mechanism during the ECDM process. Various researchers have investigated the effect of electrolyte concentration on primary process outcomes of the ECDM process. However, the published work does not provide a detailed discussion correlating the percentage deposition and the process outcomes at different electrolyte concentrations.

Experiments were conducted with the ECDM and EI-ECDM processes at 12, 20, and 28 wt.% of electrolyte concentration, while other parameters were maintained at a fixed level and selected from Table I. The experimentally obtained adequate value of applied voltage and T_{on} were fixed at 54 V and 4 ms. Gradual increment in the percentage deposition of the machined by-process on tool-electrode with increasing electrolyte concentration can be observed from Fig. 17. The fact behind this can be attributed to the formation of more machined by-products at higher electrolyte concentrations. Besides, the increasing electrolyte concentration also increases electrical conductivity in the ECDM circuit as well as chemical

etching. Thus, maximum HPD can be observed in Fig. 18b at 28 wt.% electrolyte concentrations. On the other hand, the effect of electrolyte concentration on HOC was different. It initially decreased till 20 wt.% then again increased at 28 wt.%, which may be referred from Fig. 18b. It may be due to the contribution of chemical action on material removal at 20 wt.% electrolyte concentration. However, unwanted acceleration in chemical action enlarged the hole diameter at 28 wt.% electrolyte concentration.

A comparison of the ECDM and EI-ECDM process performance can also be seen in Figs. 17 and 18. It may be noticed from Figs. 17 and 18, the EI-ECDM process with controlled delivery of electrolyte into the tooltip augmented both the process outcomes (i.e., HOC and HPD) with lower percentage deposition of machined by-products on tool-electrode. Controlled electrolyte delivery replenished the localized zone's vaporized electrolyte, thus maintaining electric discharges from the tooltip led to lower percentage deposition. It further lowered down the joule heating and subsequent electrolyte vaporization. Consequently, the emergence of electric discharges at the tooltip rather than the hole entrance increased HPD and reduced the HOC during the EI-ECDM process.

Moreover, the evidence of the experimental results is illustrated in Fig. 19 by microscopic images of tooltips and holes at different electrolyte concentrations. As shown, a shallow hole with a thermally damaged edge was produced at 12 wt.% electrolyte concentration due to the poor chemical etching action in both processes. Further, increasing the electrolyte concentration to

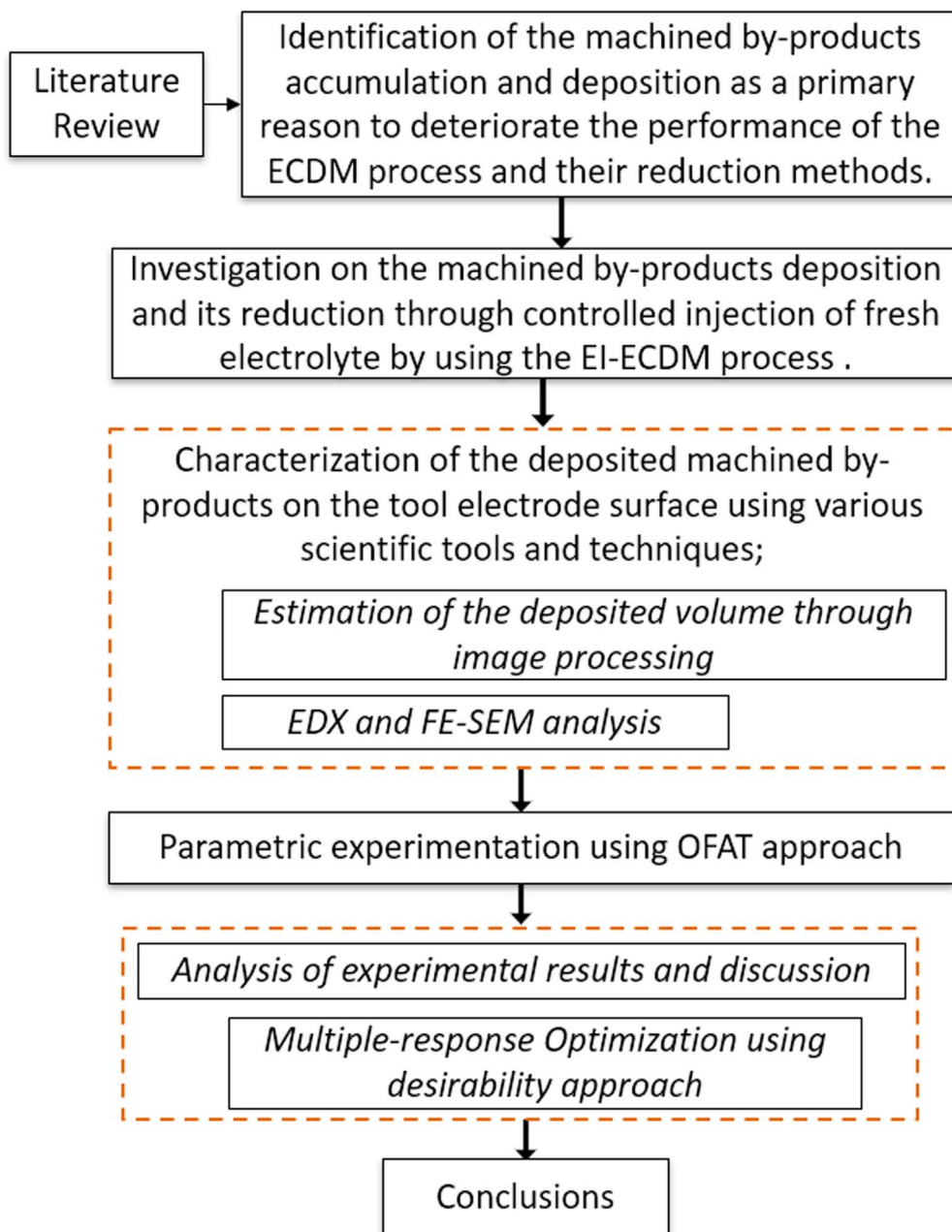


Figure 21. Summary of the present work.

20 wt.% improved the hole morphology by accelerating the chemical action. However, the process machined holes with larger entrance diameters due to unwanted chemical action at 28 wt.% electrolyte concentrations. Meanwhile, the microscopic images show the improved morphology of holes machined using the EI-ECDM process for all the levels of electrolyte concentration. The fact can be justified as stabilizing electric discharges at the tooltip by providing an adequate amount of electrolyte through tubular tool-electrode. It results in less machined by-products formation at tooltip leads to lower localized electrolyte vaporization and deposition at tool-electrode. It was due to the reduced joule heating. Microscopic images of tool-electrodes with deposited machined by-products can also be seen in Fig. 19.

It can be seen that the EI-ECDM process provided better outcomes as compared to the ECDM process during the hole machining of borosilicate glass. Also, the above parametric investigation gives information only about the effect of individual process parameters on

an individual process outcome. However, optimization of process parameters by considering the multiple process outcomes is essential to increase the applicability of the process. Thus, in the next section, the Multiple response optimization was performed on the EI-ECDM process by using the desirability approach.

Multiple response optimization.—Multi-response optimization (MRO) was executed on the experimental results obtained from the EI-ECDM process. The experimental results of the EI-ECDM process are given in Table II. The desirability function method suggested by Harrington and later strengthened by Derringer and Suich was adopted for MRO. In this method, normalization (i.e., between 0–1) of each response variable Y_i was carried out to obtain the desirability value D_i for each Y_i . The D_i is a function of the “desirability” of the corresponding Y_i .

If the value of desirability is zero, it refers to an undesirable response. On the contrary, desirability value one is a fully desired

response. Thus, D_i for each desire response (i.e., *higher the better* and *lower the better*) can be evaluated with the help of the following equations:

For *higher the better*, individual desirability can be expressed as;

$$d_i = \begin{cases} 0 & Y_i \leq Y_{\min} \\ \{(Y_i - Y_{\max}) / (Y_{\max} - Y_{\min})\}^r & Y_{\min} < Y_i < Y_{\max} \\ 1 & Y_i \geq Y_{\max} \end{cases}$$

For *lower the better*, individual desirability can be expressed as;

$$d_i = \begin{cases} 0 & Y_i \leq Y_{\min} \\ \{(Y_{\max} - Y_i) / (Y_{\max} - Y_{\min})\}^r & Y_{\min} < Y_i < Y_{\max} \\ 1 & Y_i \geq Y_{\max} \end{cases}$$

where, Y_{\min} = minimum acceptable of Y_i , Y_{\max} = maximum acceptable of y_i . Also, The desirability function's shape is a function of r , which lies between 0.1 to 10. Besides, $r > 1$ indicates the specific desired goal. Subsequently, the overall desirability of the process can be calculated as,

$$d = (d_1 \times d_2 \times d_3 \dots \dots \times d_k)^{1/k}$$

where, K represents the number of responses.

Moreover, the MINITAB-19 software package was used to perform the MRO on EI-ECDM's process parameters. The MRO was aimed to minimize the percentage deposition and HOC, whereas HPD was to maximize. Here, the desirability criteria were applied like *lower the better* for deposition and HOC and *higher the better* for HOC. As per the desired machining of the hole, both quality outcomes (i.e., percentage deposition and HOC) and productivity outcome HPD are equally imperative. Thus equal weightage was set for all the response variables.

Figure 20 shows the estimated optimized value of each response variable with the corresponding desirability. The minimum HOC and percentage deposition, and maximum HPD were estimated to be 93 μm , 7.87%, 823 μm respectively at optimal parameters of applied voltage 54 V, T_{on} 2 ms, electrolyte concentration 23 wt.%. The optimum values of the ECDM's process parameters were obtained using the desirability approach to achieve maximum HPD, minimum percentage deposition, and HOC. Then, confirmatory experiments are performed for validation of optimal values. This set of experiments is repeated thrice, and finally, the average value was taken as the final value.

The set of confirmatory experiments produces very close results to optimized results with an 8% of average error.

Eventually, Fig. 21 can be referred to the present work's summary. Herein, the typical workflow (i.e., followed in the present research work) is depicted.

Conclusions

In the present work, a set of experiments was performed to understand the consequence of the machined by-products deposition on the process performance of the ECDM and EI-ECDM processes. OFAT approach was used for the experiments. Scientific tools and techniques were used to explore the underlying phenomenon of deposition and its possible effects on the ECDM's performance.

Some main conclusions were drawn from the experimental results, which are as follows;

- Continuous machining with ECDM formed the machined by-products (i.e., sludge, debris, and salt), which critically lowered down the performance of the ECDM process after 8 min of machining owing to excessive deposition (evidenced in FE-SEM images) over the tool electrode.

- EDX analysis revealed that deposition of the machined by-products over the tool surface could alter the tool geometry, surface texture, and electrical properties. Hence, the performance of the ECDM process deteriorated.

- Further, it was observed in the parametric investigation that higher applied voltage, T_{on} , and electrolyte concentration results in more deposition during both the processes (i.e., ECDM and EI-ECDM). Meanwhile, the EI-ECDM with controlled fresh electrolyte injection to the tooltip significantly reduced the consequences of deposition.

- Moreover, the multiple response optimization (MRO) was performed for the EI-ECDM process. The MRO results showed 54 V applied voltage, 2 ms T_{on} , and 23 wt.% electrolyte concentration provided maximum HPD and minimum HOC and % deposition for the given parametric range.

- The present investigation provided insights into the deposition phenomena of machined by-products and their consequences on ECDM performance. Thus future research may be focused on the proper elimination of machined by-products from the machining zone.

ORCID

Rajendra Kumar Arya  <https://orcid.org/0000-0002-5566-3894>

References

1. C. K. Yang, C. P. Cheng, C. C. Mai, A. C. Wang, J. C. Hung, and B. H. Yan, *Int. J. Mach. Tools Manuf.*, **50**, 1088 (2010).
2. R. K. Arya and A. Dvivedi, *J. Mater. Process. Technol.*, **266**, 217 (2019).
3. Y. Zhang, J. Tang, Y. Wang, Q. Ni, and L. Ji, *Int. J. Electrochem. Sci.*, **14**, 11663 (2019).
4. M. Harugade, S. Waigaonkar, and N. Mane, *Mater. Today Proc.*, **5**, 17188 (2018).
5. T. Singh, R. K. Arya, and A. Dvivedi, *Mach. Sci. Technol.*, **24**, 195 (2020).
6. T. Singh and A. Dvivedi, *Int. J. Mach. Tools Manuf.*, **105**, 1 (2016).
7. N. Kumar, N. Mandal, and A. K. Das, *Mater. Manuf. Process.*, **35**, 363 (2020).
8. V. Rajput, M. Goud, and N. M. Suri, *J. Electrochem. Soc.*, **168**, 013503 (2021).
9. J. West and A. Jadhav, *J. Micromechanics Microengineering*, **17**, 403 (2007).
10. R. Wuthrich and J. D. A. Ziki, *Micromachining Using Electrochemical Discharge Phenomenon Fundamentals and Application of Spark Assisted Chemical Engraving* (William Andrew, Norwich, NY, United States) 2nd. ed., p. 218 (2014).
11. S. Elhami and M. R. Razfar, *J. Manuf. Process.*, **50**, 192 (2020).
12. R. K. Arya and A. Dvivedi, *Advances in Unconventional Machining and Composites* (Springer, Singapore) p. 313 (2020).
13. Y. Zhang, Z. Xu, Y. Zhu, and D. Zhu, *J. Mater. Process. Technol.*, **231**, 38 (2016).
14. T. Singh and A. Dvivedi, *Mater. Manuf. Process.*, **33**, 462 (2018).
15. H. K. Kannoija, J. Arab, B. J. Pegu, and P. Dixit, *J. Electrochem. Soc.*, **166**, D531 (2019).
16. M. Mousa, A. Allagui, H. D. Ng, and R. Wuthrich, *J. Micromechanics Microengineering*, **19**, 015010 (2008).
17. A. Behroozfar and M. R. Razfar, *Mater. Manuf. Process.*, **31**, 574 (2016).
18. N. Sabahi and M. R. Razfar, *Int. J. Adv. Manuf. Technol.*, **95**, 643 (2018).
19. D. K. Mishra, A. K. Verma, J. Arab, D. Marla, and P. Dixit, *J. Micromechanics Microengineering*, **29** (2019).
20. P. K. Gupta, *J. Electrochem. Soc.*, **165**, E279 (2018).
21. S. Kumar and A. Dvivedi, *Mater. Manuf. Process.*, **34**, 475 (2019).
22. R. K. Arya and A. Dvivedi, *IOP Conf. Ser. Mater. Sci. Eng* **647** (2019).
23. Y. Zhang, Z. Xu, J. Xing, and D. Zhu, **10**, 8465 (2015).
24. J. Zhang, Z. Xu, and C. Zhang, *Int. J. Adv. Manuf. Technol.*, **110**, 2815 (2020).
25. L. D. Paul, M. J. Danielson, S. L. Harper, and J. L. Barna, *Tappi Journal; (United States)*, **76**, 8 (1993).